Available online at www.sciencedirect.com
SCIENCE DIRECT®
PERGAMON
International Journal of Multiphase Flow 29 (2003) 1583–1604
International Journal of Multiphase Flow
www.elsevier.com/locate/ijmulflow

Stratified laminar countercurrent flow of two liquid phases in inclined tubes

A. Ullmann [a], M. Zamir [a], Z. Ludmer [b], N. Brauner [a,*]

[a] *Department of Fluid Mechanics and Heat Transfer, The Faculty of Engineering, Tel Aviv University, Tel Aviv 69978, Israel*
[b] *Faculty of Agriculture, Hebrew University of Jerusalem, Rehovot 76100, Israel*

Received 3 October 2002; received in revised form 17 July 2003

Abstract

The effects of inclination on the characteristics of laminar countercurrent liquid–liquid flow are investigated both experimentally and theoretically. Experimental results show that with a slight off-vertical inclination the phases tend to segregate and the basic flow pattern in inclined tubes is stratified flow. Moreover, for fixed operational conditions, there exist two stable modes of stratified configuration that differ in the in situ holdup, velocity profiles and the pressure drop, and both may co-exist in the column. The application of the two-fluid and the two-plate models for the prediction of the characteristics of countercurrent flow is explored. Both models predict the existence of the two modes that have been observed in the column and their associated holdups. The TP model confirms the experimental finding that back flow (opposite to the feed direction) is an inherent characteristic of countercurrent flow and generally, is expected in the thicker layer. The findings of this study are applicable for improving the throughput of phase transition extraction columns.

Keywords: Countercurrent; Holdup; Inclined; Liquid–liquid; Oil-water; Stratified

1. Introduction

Countercurrent flows of immiscible fluids are encountered frequently in the design of industrial processes such as liquid–liquid extraction (LLE). The LLE process has important applications in

* Corresponding author. Tel.: +972-3-640-3127; fax: +972-3-640-7334.
E-mail address: brauner@eng.tau.ac.il (N. Brauner).

0301-9322/$ - see front matter
doi:10.1016/S0301-9322(03)00144-7

many industries and has been extensively studied (Treybal, 1963; Lo et al., 1983; Robbins and Roger, 1997). In a single stage of LLE process, the droplets of one phase are initially dispersed in a second phase to facilitate mass-transfer of the solute across the liquid–liquid boundary and then the two mixed phases are separated. Basically, there are two types of multi-stage contact equipment. Those where each individual stage is a separate unit (mixer-settler), and those in which several stages are integrated into one column.

A novel and promising extraction process termed phase transition extraction (PTE) (Ullmann et al., 1995; Ullmann et al., 1997) introduced a different approach to conventional extraction processes. The PTE process is based on the use of a class of solvents that have a critical solution temperature (CST) with the feed liquid. In the PTE column, heating and cooling sections replace the mixing and settling sections of conventional extraction columns. The countercurrent feed and solvent streams passing those sections are heated and cooled across their coexistence curve and thereby undergo phase transitions, which alternate between immiscible and miscible liquid phases. With a formation of a single phase in the mixing section a substantially superior contact between the solvents is achieved. As explained in Ullmann et al. (1995), the continuous change in the composition of the phases during the cooling and the phase separation process prevents the formation of a stable emulsion. Consequently, the coalescence process is very fast, and the process is not sensitive to the presence of impurities or emulsifiers.

For all practical purposes, the time scale and therefore the throughput of extraction columns, as well as the PTE column is dominated by the settling section. Although, the coalescence in the PTE process is very rapid, the maximal flow rates in the settling section are determined by flooding limitations. Postponing the flooding, and thereby improving the column performance, can be accomplished in off-vertical inclined settlers.

Available experimental data on countercurrent liquid–liquid (LL) inclined flows are limited to those obtained by Johnston (1984) for liquids with a density ratio of 0.25. Obviously, the density ratio is one of the controlling parameters in inclined two-phase flow. This ratio in the air/water case is of the order of 10^{-3}. In extraction processes this parameter gets a characteristic value between 0.75 and 1. More information concerning the various aspects related to the characteristics of countercurrent flow of two immiscible liquids of low density-difference is required.

Experimental results obtained in the present study (Section 2) show that with a slight off-vertical inclination the phases tend to segregate. Hence, stratified flow is to be considered as a basic flow pattern in inclined LL countercurrent flows. Moreover, for fixed operational conditions, there exist two different stable modes of stratified configuration and both may co-exist in the column.

The feasibility of obtaining two stable modes in inclined countercurrent flows is proved also via investigation of the exact solutions obtained for the model of laminar flow through inclined plates and via the solutions of a two-fluid model for countercurrent flow in pipes (Section 3). The model equations are presented in a unified form, applicable both to countercurrent and co-current flows. For co-current inclined flows, these models yield non-unique solutions for some *upward* inclined and *downward* inclined flows. In this paper the solution space in countercurrent flows is investigated in terms of the controlling non-dimensional parameters in gas–liquid and liquid–liquid systems and compared with experimental results. The investigation of multi-valued holdup in co-current stratified flows in inclined tubes is the subject of the following paper (Ullmann et al., 2003).

2. Experiments

2.1. Experimental system

The solvent system used in this study is a mixture of ethyl acetate, water and ethanol with an upper critical solution temperature (UCST) of 42 °C. At room temperature, this solvent system forms two phases with a density ratio of $\rho_o/\rho_w \approx 0.95$, viscosity ratio of $\mu = \mu_w/\mu_o \approx 1.7$ and surface tension $\sigma \approx 0.004$ N/m, where subscript 'w' denotes the heavy (water-rich) phase and 'o' denotes the light (organic-rich) phase. The corresponding Eotvos number of the system is $Eo = \Delta\rho g D^2/\sigma \approx 20 \gg 1$ hence, the system is gravity dominated. It is to be noted that some changes in the mixture composition and temperature between different runs cause a variation of the phases' physical properties (in the range of $\Delta\rho/\rho_w = \pm 0.02$ and for the viscosity ratio, $\Delta\mu = \pm 0.25$).

A schematic description of the flow system and the auxiliary equipment are depicted in Fig. 1a. The test column is mounted on a support system, which permits any inclination between 0° and 90° to the horizontal. The entry devices used to introduce the liquids into the test section are designed to minimize entrance disturbances. The liquids flow under gravity from two feed reservoirs through a set of calibrated rotameters (Gilmont calibrated/correlated flow meters with an

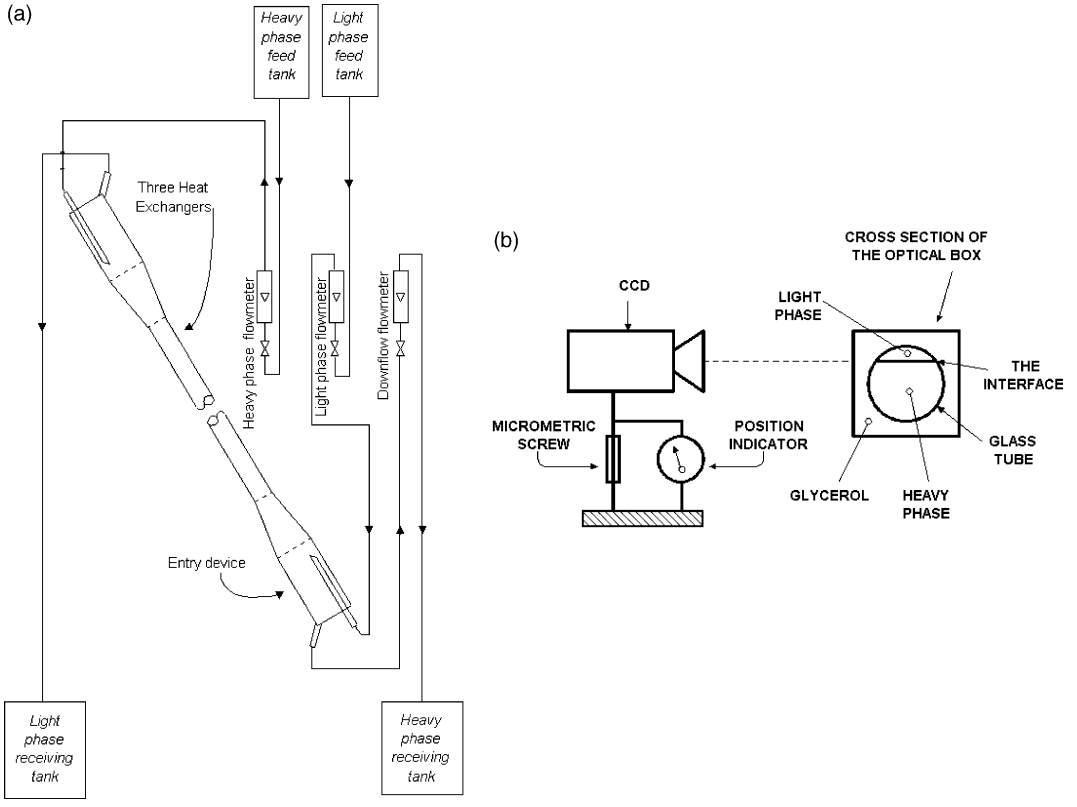

Fig. 1. Schematic description of the experimental setup: (a) the flow system, (b) visualization setup.

accuracy of ±2%) into the test section, and collected back in two storage tanks. The latter are used also as liquid separators.

Needle valves are used to control the liquids flow rates (Gilmont micrometer valve, 20 turns with Teflon O rings) and pressure transducers for measuring the pressure drop. The heavy phase is introduced at the column's upper end and removed from the bottom, through an additional set of control valve and a rotameter, back into its storage tank. The light phase overflows from the top of the column into the light phase storage tank.

The test column consists of a one-meter length, 14.4-mm I.D. Pyrex pipe (Duran) with a wall thickness of 1.8 mm. The entry sections at the column top and bottom are identical; these sections are 140 mm long, where the first 80-mm were shaped as a cylinder (32 mm I.D.), the rest was shaped as an entry cone. The heavy phase and light phase are introduced through the inlet tubes (6-mm I.D. by 60 mm long), which are located near the wall parallel to the column axis.

It is worth noting that the top of the column is at atmospheric pressure. The pressure difference between the column top and bottom is due to wall friction and hydrostatic head. This pressure difference must be balanced by an appropriate adjustment of the control valve resistance located on the heavy phase exit line. For maintaining constant flow rates, any change of the column inclination must be accompanied with a proper adjustment of this valve to compensate for the change in the pressure drop along the column. The ranges of light and heavy phase flow rates tested is 0–50.8 ml/min and 0–77.7 ml/min, respectively. The maximal liquids flow rates correspond to Reynolds number less than 100, hence all data correspond to laminar flow.

The flow patterns and the location of the interface are identified and recorded using a commercial camera (Panasonic NV-RX11EN/EU) with a recording resolution of 625 lines, 50 fields PAL color signal, optical capability of 21:1 wide angle power zoom lens and focal length: 3.8–79.8 mm. The camera is mounted on a support with a height adjustment mechanism. The camera position is indicated by a dial of 5 mm full scale, with 0.01-mm graduations. The camera was first positioned to have its focus on the inner tube wall and then moved to a second position to have its focus on the interface. The difference between these positions provides a measure of the heavy (or light) layer thickness (see also Zamir, 2003). In order to avoid optical distortion, the inclined column is placed within a rectangular optical box. The optical box was made of 4-mm Perspex plates and is filled with pure Glycerol. A detailed description of the visualization setup is given in Fig. 1b.

In order to obtain easy identification of the interface level, a striped background (white/pink, 5 mm wide) was placed behind the optical box. A distortion of stripes indicates the location of the liquid–liquid interface. Illumination by incandescence lamps (positioned above and below the optical box) was reflected from the white strips through the optical box to the camera lens. Validation of the holdup measurement technique (which is based on the above measurement of the interface level) was carried out by comparing the measured value of the holdup in a sealed tube filled with known liquid volumes. The relative error in the holdup is evidently higher for thinner layers, however, the relative error was less than 1%. In the flow system, the establishment of fully developed conditions was verified by taking measurements of the holdup at several locations along the middle section of the pipe (30 cm downstream the entry sections). In all cases, the variations of the holdup were random and limited to the measurement error range (less than the marks size in the figures).

To observe the velocity field, the liquids were seeded with small amount of tracer particles (concentration of 1.32 Mg/cm^3, hollow spherical non-porous glass beads, diameter 0.01 mm, density 1.1 gr/cm^3) and a light sheet illumination normal to the camera axis was used. Quantitative information of the velocity field was obtained by employing a standard particle image velocimetry (PIV) technique. The interrogation area for most of the measurements was set at 32×32 pixels (for high velocity—64×64 pixels) with a time interval of 1/25 s between two successive frames. Further details on the experimental setup are provided in Zamir (2003).

2.2. Experimental results

Fig. 2 shows a schematic description of the flow patterns obtained in the column for countercurrent flow of relatively low flow rates of the light and heavy phases. Pictures reproduced from the video film are given in Fig. 3, showing the flow pattern in the column. In a vertical column (Figs. 2a and 3a, b), the basic flow pattern is dispersed flow, with either the heavy phase dispersed in the light phase (light phase dominated, LPD), or the light phase dispersed in the heavy phase (heavy phase dominated, HPD). These two configurations of dispersed flow can be simultaneously obtained in the column, separated by an interface. Obviously, each of the two modes is associated with a different in situ holdup and thus, with a different pressure gradient. Therefore, by manipulating the resistance at the heavy phase outlet, the location of the interface between the LPD and the HPD zones can be placed at any position along the column. With a sufficiently low resistance, the flow pattern in the entire column is LPD (the interface is out of the column bottom). On the other hand, with a high resistance, the flow pattern is entirely HPD (the interface is out of the column top). When the interface is set within the column, the HPD mode prevails at the lower section of the column, while in the upper section, the LPD mode is obtained (see also the description of countercurrent vertical spray column in Treybal, 1963, p. 473).

With a slight off-vertical positioning of the column (Figs. 2b and 3c,d), the phases tend to segregate, even with the liquids of the small density differential used in this study. The two configurations obtained in this case correspond to stratified-dispersed flow both in the HPD and in the LPD zones. Further inclining the tube results in a complete segregation of the phases. In an inclined tube (Fig. 2c), the basic flow pattern in both zones is stratified flow with either a wavy

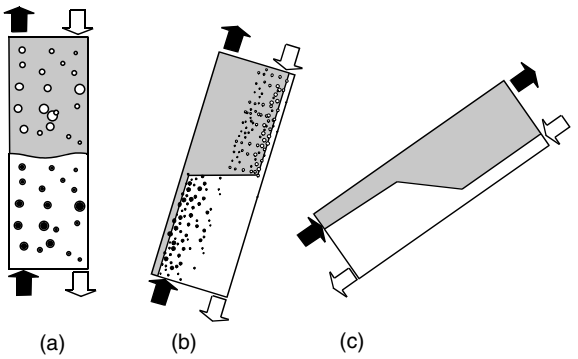

Fig. 2. Description of the flow pattern in countercurrent flow: (a) vertical, (b) off-vertical, (c) inclined column.

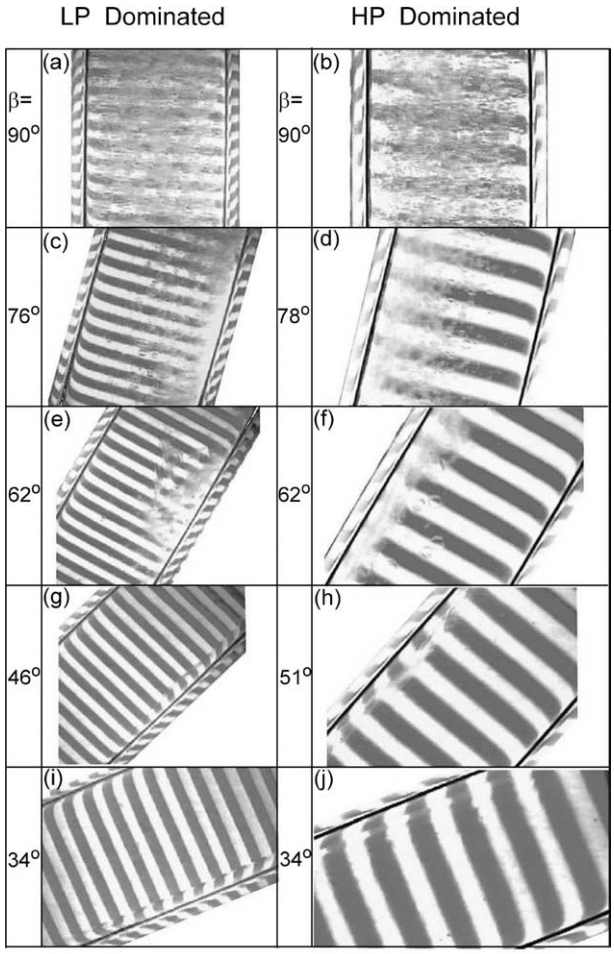

Fig. 3. Pictures showing the flow patterns obtained in the LPD and HPD zones at different column inclinations.

(Fig. 3e–h) or smooth interface (Fig. 3i,j). The flow in the HPD zone corresponds to a thick layer of the heavy phase flowing countercurrently to a thin layer of the light phase, while in the LPD a thin layer of the heavy phase is obtained. Similarly to the operation of a vertical column, the location of the interface between these two zones can be controlled by adjusting the resistance at the heavy phase outlet. Thereby, the entire column can be occupied by either one of these two flow configurations, or by both of them.

3. Modeling

The characteristics of countercurrent stratified flow are analyzed using two simple models. The first model is for laminar two-phase flow between two parallel inclined plates and the second is the

two-fluid model for pipe geometry. The models equations are presented in a unified form that is applicable both to co-current and countercurrent stratified flows.

3.1. Two-plates model

The flow geometry is schematically described in Fig. 4. The feed flow rates of the heavy and light phases (per unit width) are q_1 and q_2 respectively and H is the distance between the plates. For laminar flow, the fully developed velocity profiles in the two layers are obtained by integrating the following two momentum equations:

$$\mu_1 \frac{\partial^2 u_1}{\partial y^2} = \frac{\mathrm{d}p}{\mathrm{d}z} - \rho_1 g \sin\beta; \quad -h \leqslant y < 0 \tag{1.1}$$

$$\mu_2 \frac{\partial^2 u_2}{\partial y^2} = \frac{\mathrm{d}p}{\mathrm{d}z} - \rho_2 g \sin\beta; \quad 0 < y \leqslant H - h \tag{1.2}$$

subjected to the following boundary conditions:

$$\begin{aligned} &u_1|_{y=-h} = 0; \quad u_2|_{y=H-h} = 0 \\ &\mu_1 \frac{\partial u_1}{\partial y}|_{y=0} = \mu_2 \frac{\partial u_2}{\partial y}|_{y=0}; \quad u_1|_{y=0} = u_2|_{y=0} \end{aligned} \tag{1.3}$$

Integration of Eqs. (1) yields the following dimensionless velocity profiles:

$$\tilde{u}_1 = \frac{u_1}{U_{1s}} = \frac{6\widetilde{P}}{\mu q}\left\{(1 - Y/\widetilde{P})\tilde{y}^2 + a\tilde{y} + \mu b\right\}; \quad -\tilde{h} \leqslant \tilde{y} < 0 \tag{2.1}$$

$$\tilde{u}_2 = \frac{u_2}{U_{2s}} = 6\widetilde{P}\left\{\tilde{y}^2 + a\tilde{y} + b\right\}; \quad 0 \leqslant \tilde{y} < 1 - \tilde{h} \tag{2.2}$$

with

$$\begin{aligned} &a = \frac{\mu(1-\tilde{h})^2 - (1 - Y/\widetilde{P})\tilde{h}^2}{\mu\tilde{h} - \mu - \tilde{h}}; \quad b = \frac{\tilde{h}(1-\tilde{h})(1 - \tilde{h}Y/\widetilde{P})}{\mu\tilde{h} - \mu - \tilde{h}} \\ &\tilde{y} = y/H; \quad \tilde{h} = h/H; \quad U_{1s} = q_1/H; \quad U_{2s} = q_2/H \\ &\widetilde{P} = \frac{\mathrm{d}p/\mathrm{d}z - \rho_2 g \sin\beta}{(-\mathrm{d}p/\mathrm{d}z)_{2s}}; \quad \mu = \mu_1/\mu_2 \\ &Y = \frac{(\rho_1 - \rho_2) g \sin\beta}{(-\mathrm{d}p/\mathrm{d}z)_{2s}}; \quad q = q_1/q_2 \end{aligned} \tag{3}$$

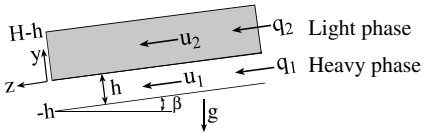

Fig. 4. Schematic description of the stratified flow configuration and coordinates, $0 \leqslant \beta \leqslant 90°$ (in countercurrent flow $q_2 < 0$ is fed at the pipe bottom and flows upward).

and $(-\mathrm{d}p/\mathrm{d}z)_{2s} = 12\mu_2 q_2/H^3$ is the superficial frictional pressure drop for single phase flow of the lighter phase. It is worth noting that for countercurrent flow q_2 is negative (the light phase flows upward), whereas for co-current flow q_1, q_2 are positive in case of downward flow and both are negative for upward flow. Mass conservation equations read:

$$\int_{-\tilde{h}}^{0} \tilde{u}_1 \,\mathrm{d}\tilde{y} = 1 \tag{4.1}$$

$$\int_{0}^{1-\tilde{h}} \tilde{u}_2 \,\mathrm{d}\tilde{y} = 1 \tag{4.2}$$

Substituting the velocity profiles, Eqs. (2), into Eqs. (4) yields the following two equations:

$$Y = \frac{1}{4}\frac{\mu q(1-\tilde{h})^2[(1+2\tilde{h})\mu + (1-\mu)\tilde{h}(4-\tilde{h})] - \tilde{h}^2[(3-2\tilde{h})\mu + (1-\mu)\tilde{h}^2]}{\tilde{h}^3(1-\tilde{h})^3[\tilde{h}+\mu(1-\tilde{h})]} \tag{5.1}$$

$$\widetilde{P} = \frac{1}{4}\frac{3\mu q(1-\tilde{h})^2 - 4\mu\tilde{h}(1-\tilde{h}) - \tilde{h}^2}{\tilde{h}(1-\tilde{h})^2[(1+2\tilde{h})\mu + (1-\mu)\tilde{h}(4-\tilde{h}) - 3\tilde{h}]} \tag{5.2}$$

Given the parameters Y, μ and q, Eq. (5.1) can be solved for the in situ holdup of the heavier phase $\tilde{h}$, which in turn can be substituted into Eq. (5.2) to obtain $\widetilde{P}$. The total pressure drop is composed of the gravitational (hydrostatic) pressure drop:

$$\left(\frac{\mathrm{d}p}{\mathrm{d}z}\right)_g = \left[\rho_1\tilde{h} + \rho_2(1-\tilde{h})\right]g\sin\beta = \left[\rho_2 + (\rho_1-\rho_2)\tilde{h}\right]g\sin\beta \tag{6}$$

and the frictional pressure drop, $(\mathrm{d}p/\mathrm{d}z)_{\mathrm{f}}$. In terms of the solution dimensionless parameters, the dimensionless frictional pressure drop, $\prod_{\mathrm{f}}$ is given by

$$\prod_{\mathrm{f}} = -\frac{\mathrm{d}p/\mathrm{d}z - (\mathrm{d}p/\mathrm{d}z)_g}{(-\mathrm{d}p/\mathrm{d}z)_{2s}} = -\widetilde{P} + Y\tilde{h} \tag{7}$$

Thus, the characteristics of stratified laminar flow of two fluids in inclined conduits are determined in terms of the three dimensionless parameters: μ, Y and q. The range of these parameters for the possible co-current and countercurrent flow configurations encountered by the model are summarized in Table 1. The expressions obtained for the various flow characteristics, which include the interfacial velocity and shear stress $(u_{\mathrm{i}}, \tau_{\mathrm{i}})$, the wall shear stress (τ_1, τ_2) are shown in Table 2. It is worth noting that consistent with the coordinate system of Fig. 4, $\tau > 0$ corresponds to a shear stress in the positive z direction.

Table 1
Range of Y and q for the various flow configurations

	$Y = \dfrac{\Delta\rho g\sin\beta}{(-\mathrm{d}p/\mathrm{d}z)_{2s}}$	q
Co-current downward	>0	>0
Co-current upward	<0	>0
Countercurrent (light phase upward)	<0	<0

Table 2
Characteristics of flow between two parallel plates

Interfacial velocity	$\tilde{u}_\mathrm{i} = \dfrac{u_\mathrm{i}}{U_{2s}} = \dfrac{6\tilde{h}(1-\tilde{h})(Y\tilde{h}-\widetilde{P})}{\mu(1-\tilde{h})+\tilde{h}}$
Interfacial shear stress (exerted by the lower phase on the upper phase)	$\tilde{\tau}_\mathrm{i} = \dfrac{\tau_\mathrm{i}}{\tau_{2s}} = \dfrac{\tilde{h}^2(\widetilde{P}-Y)-\mu\widetilde{P}(1-\tilde{h})^2}{\mu(1-\tilde{h})+\tilde{h}}$; $\tau_{2s} = \dfrac{6\mu_2 q_2}{H^2}$
Lower wall shear stress	$\tilde{\tau}_1 = \dfrac{\tau_1}{\tau_{1s}} = \dfrac{(1-\tilde{h})[\mu\widetilde{P}(1+\tilde{h})-2Y\mu\tilde{h}]+\tilde{h}^2(\widetilde{P}-Y)}{q\mu[\mu(1-\tilde{h})+\tilde{h}]}$; $\tau_{1s} = \dfrac{6\mu_1 q_1}{H^2}$
Upper wall shear stress	$\tilde{\tau}_2 = \dfrac{\tau_2}{\tau_{2s}} = \dfrac{\widetilde{P}[(1-\tilde{h})^2(\mu-1)+1)]-\tilde{h}^2 Y}{\mu(1-\tilde{h})+\tilde{h}}$

3.2. Two-fluid model

The integral forms of the momentum equations for the two fluids in stratified flow are

$$-A_1\frac{\mathrm{d}p}{\mathrm{d}z} + \tau_1 S_1 - \tau_\mathrm{i} S_\mathrm{i} + \rho_1 A_1 g\sin\beta = 0 \tag{8.1}$$

$$-A_2\frac{\mathrm{d}p}{\mathrm{d}z} + \tau_2 S_2 + \tau_\mathrm{i} S_\mathrm{i} + \rho_2 A_2 g\sin\beta = 0 \tag{8.2}$$

where $A_{1,2}$ and $S_{1,2}$ are the cross-sectional area and the wall perimeter of each of the fluids respectively, S_i is the interfacial perimeter and τ_1 and τ_2 are the average shear stresses around their respective peripheries. Eliminating the pressure drop yields:

$$\tau_1\frac{S_1}{A_1} - \tau_2\frac{S_2}{A_2} - \tau_\mathrm{i} S_\mathrm{i}\left(\frac{1}{A_1}+\frac{1}{A_2}\right) + (\rho_1-\rho_2)g\sin\beta = 0 \tag{9}$$

Exact computation of the velocity profiles and the resulting wall and interfacial shear stresses is limited to laminar flows and simple geometries (i.e. Tang and Himmelblau, 1963; Bentwich, 1964; Brauner et al., 1996). For pipe flows, the practical approach is to introduce closure laws for the average shear stresses in terms of the average velocities of the fluids (U_1, U_2) and appropriate friction factors (f_1, f_2, f_i):

$$\tau_1 = -\frac{1}{2}\rho_1 f_1 U_1|U_1|; \quad f_1 = c_1\left(\frac{\rho_1 D_1|U_1|}{\mu_1}\right)^{-n_1} \tag{10.1}$$

$$\tau_2 = -\frac{1}{2}\rho_2 f_2 U_2|U_2|; \quad f_2 = c_2\left(\frac{\rho_2 D_2|U_2|}{\mu_2}\right)^{-n_2} \tag{10.2}$$

$$\tau_\mathrm{i} = -\frac{1}{2} f_\mathrm{i}\rho(U_2-U_1)|U_2-U_1| \tag{10.3}$$

Equivalent hydraulic diameters (D_1 and D_2) are used to evaluate the Re numbers in each of the layers, and for laminar flow in both phases the constants are $c_{1,2} = 16$ and $n_{1,2} = 1$. However, the above commonly used relations ignore possible effects of the flow geometry and the interaction between the flow in the two layers on the structure and parameter values of the closure laws.

The mass balances yield:

$$\widetilde{U}_1 = \frac{U_1}{U_{1s}} = \frac{\pi}{4}\widetilde{A}_1^{-1} \tag{11.1}$$

$$\widetilde{U}_2 = \frac{U_2}{U_{2s}} = \frac{\pi}{4}\widetilde{A}_2^{-1} \tag{11.2}$$

where U_{1s}, U_{2s} are the superficial phases velocities. Eqs. (8)–(11) are applicable both for co-current and countercurrent flows. The geometrical relationships for $\widetilde{A}_{1,2}$, $\widetilde{S}_{1,2}$ and $\widetilde{S}_i$ ($\sim$ denotes normalized variables, area by D^2 length by D) are given in terms of $\tilde{h}$ for a plane interface (Taitel and Dukler, 1976) and for curved interface in terms of the interface curvature (Brauner et al., 1998). The definition of the hydraulic diameters D_1, D_2, used in Eqs. (10.1) and (10.2), requires some adjustment according to the relative velocity of the two layers. For co-current (upward or downward) flows the following definitions are used (Brauner and Moalem Maron, 1989):

$$D_2 = \frac{4A_2}{(S_2 + S_i)}; \quad D_1 = \frac{4A_1}{S_1} \quad \text{for } |U_2| > |U_1| \tag{12.1}$$

$$D_2 = \frac{4A_2}{S_2}; \quad D_1 = \frac{4A_1}{(S_1 + S_i)} \quad \text{for } |U_2| < |U_1| \tag{12.2}$$

$$D_2 = \frac{4A_2}{S_2}; \quad D_1 = \frac{4A_1}{S_1} \quad \text{for } |U_2| \simeq |U_1| \tag{12.3}$$

In countercurrent flow, each of the layers is dragged by the other one opposite to its flow direction, therefore:

$$D_2 = \frac{4A_2}{S_2 + S_i}; \quad D_1 = \frac{4A_1}{S_1 + S_i} \tag{13}$$

In co-current the interfacial friction is commonly estimated as equal to the wall friction factor of the faster layer, thus:

$$\begin{aligned} &\rho = \rho_2 \quad \text{and} \quad f_i = f_2 \quad \text{for } |U_2| > |U_1| \\ &\rho = \rho_1 \quad \text{and} \quad f_i = f_1 \quad \text{for } |U_1| > |U_2| \\ &\tau_i \simeq 0 \quad \text{for } U_2 \simeq U_1 \end{aligned} \tag{14}$$

The applicability of Eq. (14) for modeling countercurrent flows will be tested below based on the experimental results. Introducing dimensionless variables and substituting Eqs. (10)–(14) into Eq. (9) yields

$$\frac{\widetilde{U}_2}{\widetilde{D}_2}\left[\frac{\widetilde{S}_2}{\widetilde{A}_2} + \left|1 - q\frac{\widetilde{U}_1}{\widetilde{U}_2}\right|\left(1 - q\frac{\widetilde{U}_1}{\widetilde{U}_2}\right)\widetilde{S}_i\left(\frac{1}{\widetilde{A}_1} + \frac{1}{\widetilde{A}_2}\right)\right] - \left[\frac{\widetilde{S}_1}{\widetilde{A}_1}\frac{\widetilde{U}_1}{\widetilde{D}_1}\right]\mu q + 4Y = 0 \quad \text{for } \frac{\widetilde{U}_2}{|q|\widetilde{U}_1} > 1 \tag{15.1}$$

and

$$\frac{\widetilde{U}_2}{\widetilde{D}_2}\frac{\widetilde{S}_2}{\widetilde{A}_2}-\frac{\widetilde{U}_1}{\widetilde{D}_1}\left[\frac{\widetilde{S}_1}{\widetilde{A}_1}-\left|\frac{1}{q}\frac{\widetilde{U}_2}{\widetilde{U}_1}-1\right|\left(\frac{1}{q}\frac{\widetilde{U}_2}{\widetilde{U}_1}-1\right)\widetilde{S}_i\left(\frac{1}{\widetilde{A}_1}+\frac{1}{\widetilde{A}_2}\right)\right]\mu q+4Y=0 \quad \text{for } \frac{\widetilde{U}_2}{|q|\widetilde{U}_1}<1 \tag{15.2}$$

where q is the flow rates ratio ($=U_{1s}/U_{2s}$) and Y is the inclination parameter (Eq. (3)):

$$Y=\frac{(\rho_1-\rho_2)g\sin\beta}{32\mu_2 U_{2s}/D^2} \tag{15.3}$$

Thus, in the case of laminar flow Eqs. (15.1) and (15.2) are quadratic equations in q and can be easily solved to obtain an explicit relation between q and $\tilde{h}$. Theses equations are applicable to co-current (upward or downward) flows as well as to countercurrent flows. The solution is dependent on the same dimensionless parameters obtained in the two-plates model, μ, q, Y. Eq. (15.1) applies to the case in which τ_i is controlled by the flow of the light phase, whereas Eq. (15.2) applies when τ_i is controlled by the flow of the heavy phase. Accordingly, the application of either of these two equations is constrained by the corresponding in situ velocities ratio. These constraints should, however, be considered as weak restrictions for the applicability range of either of these equations. A relaxation of these constraints means that solutions obtained with the interfacial shear stress controlled by the slower layer are also considered. As will be shown below, such an extension of the applicability range of either of these two equations is, in some cases, required for bridging between the two solution branches.

Note that the Martinelli parameter, $X^2=(\mathrm{d}p_f/\mathrm{d}z)_{1s}/(\mathrm{d}p_f/\mathrm{d}z)_{2s}$ is equal to μq in the case of laminar flow in both layers, and thus it can replace either μ or q. The literature for gas–liquid systems, following the Lockhart and Martinelli approach (1949), emphasizes the role of X^2 and Y as the two relevant parameters that determine the holdup and pressure drop in stratified flows. Indeed, this is the case in horizontal and upward co-current gas–liquid stratified flows, where the gas velocity is typically much greater than the liquid phase velocity. However, in the general case of inclined flows, countercurrent flows and liquid–liquid systems, where velocities of the two-phases are of comparable values, the flow characteristics of two-fluid systems are dependent on three parameters, q, X^2 and Y.

Given these three dimensionless parameters (and the flow regime in each of the two layers), the solution of Eqs. (15) yields the in situ flow geometry; namely, the heavier layer thickness $\tilde{h}$ in case of plane interface (or wall perimeter wetted by the heavier phase in a case of a curved interface, Brauner et al., 1998). Once such a solution has been obtained, the in situ holdup can be calculated from geometrical relationships and the corresponding pressure drop from the sum of Eqs. (8.1) and (8.2). The dimensionless frictional pressure drop is given by

$$\prod_f=\frac{1}{\pi}\left[\left(\widetilde{S}_1\frac{\widetilde{U}_1}{\widetilde{D}_1}\right)\mu q+\widetilde{S}_2\frac{\widetilde{U}_2}{\widetilde{D}_2}\right] \tag{16}$$

4. Results and discussion

The two-plate (TP) and the two-fluid (TF) models described in Section 3 are used for studying the stratified countercurrent flow characteristics in inclined pipes. These models are applied for the

case of a plane (rather than curved) interface, as the two-fluid system used in the experimental study corresponds to a gravity dominated system of $Eo \gg 1$.

Fig. 5 shows the experimental results of the heavy phase holdup obtained for countercurrent flow in a 30° inclined tube. The data was obtained at a constant flow-rate of the heavy phase, therefore the results in the figure are shown versus the inverse of the Martinelli parameter $(1/X^2)$ and at a constant inclination parameter $(Y/X^2 = 50 \pm 2.5)$. The variation in Y/X^2 reflects errors in measured values of physical properties, flow rates and tube inclinations. The corresponding changes in the predicted holdups are approximately represented by the line thickness. All the results correspond to a stable interface namely, smooth stratified flow configuration. These results are compared with the predictions of the TP model (Fig. 5a) and the TF model (Fig. 5b). Both of the models successfully predict the existence of two different holdups for a specified flow-rate of

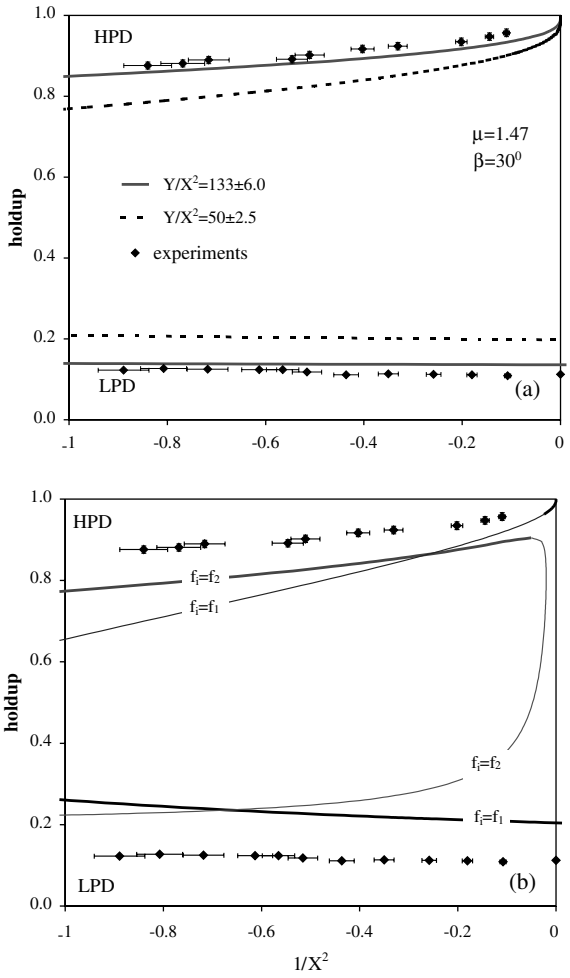

Fig. 5. Comparison of measured holdups in the HPD and LPD zones with theory for: $\beta = 30°$, $Q_1 = 45 \pm 1.5$ ml/min, $\rho_1 = 943.6$ kg/m^3, $\rho_2 = 919.7$ kg/m^3, $\mu = 1.47$ and $\mu_1 = 3.32 \times 10^{-3}$ kg/m/s: (a) TP model, (b) TF model (bold lines—$f_i = f_2$ for $|U_2| > |U_1|$ and $f_i = f_1$ for $|U_1| > |U_2|$).

the light-phase flowing countercurrently to the heavy phase. The results of the TP model are calculated with H = D using two values of the inclination parameter. One is the same as in pipe flow (corresponding to the same superficial frictional pressure drop). The second is $Y/X^2 = 133 \pm 6$, which is the value obtained when it is based on the same superficial velocity of the heavy-phase as in the pipe. As shown in the Fig. 5a, the latter is in better agreement with the data. Note that the comparison between the TP and pipe geometries is for the holdups and not for the corresponding $\tilde{h}$. A comparison based on the latter indicates less favorable agreement.

Applying the TF model for the prediction of the holdup is more problematic. The complication evolves from the inherent inaccuracy of this model in evaluating the wall shear stresses and, in particular, the interfacial shear stress. Fig. 5b shows the solutions obtained via Eqs. (15.1) and (15.2). In principle, each of these equations can provide up to two solutions for the holdup in countercurrent flow. It is worth recalling that Eq. (15.1) evolves for τ_i that is controlled by the flow of the light phase ($f_i = f_2$), whereas Eq. (15.2) is for τ_i controlled by the flow of the heavy-phase, ($f_i = f_1$). Accordingly, the segments of the holdup curves, where the velocity of the phase that controls τ_i is higher than the other phase, are marked as bold lines. For the configuration of a thin heavy phase layer, Eq. (15.2) applies for the whole range studied, whereas for the thick layer configuration Eq. (15.1) applies in most of the studied range, except for small values of $1/|X^2|$. In this range Eq. (15.2) is valid again. It is worth noting that in this range of $1/X^2 \to 0$, Eq. (15.1) does not yield any solution. Inspection of Fig. 5b indicates that, generally, the data are better represented by the 'valid' branches of the TF model solutions, however not better than the prediction of the TP model.

The above conclusions are further substantiated in view of Fig. 6, which shows the results obtained for a shallow inclination of $\beta = 5.5°$ (constant q_1 corresponding to $Y/X^2 = 18 \pm 1.6$ in pipe). While the TP model (Fig. 6a) yields a reasonable prediction for the holdup both in the HPD and the LPD zones, the predictions of the TF model (Fig. 6b) are poor. In addition, as can be seen in Figs. 5b and 6b, there is a range of flow rates where four solutions coexist. Adopting a criterion based on the ratio of the absolute phase velocities for switching between the solutions of Eqs. (15.1) and (15.2) (as implied by the results in Fig. 5b), reduces the number of solutions, but introduces a discontinuity in the TF model prediction. Moreover, there is a range of flow rates where this model does not provide any solution. Since the prediction of the holdup in the LPD zone via Eq. (15.2) is limited to small values of $1/|X^2|$ (<0.416), an extension of Eq. (15.1) to the range where $U_1 > U_2$ is required to bridge the gap between the two solution branches ($f_i = f_2$ is valid until point Q). A similar extension is required also in the HPD zone ($f_i = f_1$ is valid until point P). However, these extensions add additional two solutions (a total of four solutions) in part of the flow rate range.

The results of applying this procedure for handling the TF model predictions in the countercurrent regime are summarized in Figs. 7 and 8. In these figures the model predictions are depicted against experimental data obtained for different flow rates (q_1 and q_2) and at various pipe inclinations. The data for the measured h/D obtained at various inclinations and flow rates are available at the authors' address upon request.

Again, Fig. 7a shows that an attempt to apply the TF model with $f_i = f_1$ (determined based of the flow of the more viscous phase) fails to give any solution for many of the experimental points (indicated by the circles on the top of the figure) and a very poor prediction of the holdup, particularly in the HPD zone. Fig. 7b shows that the prediction for the HPD zone is definitely

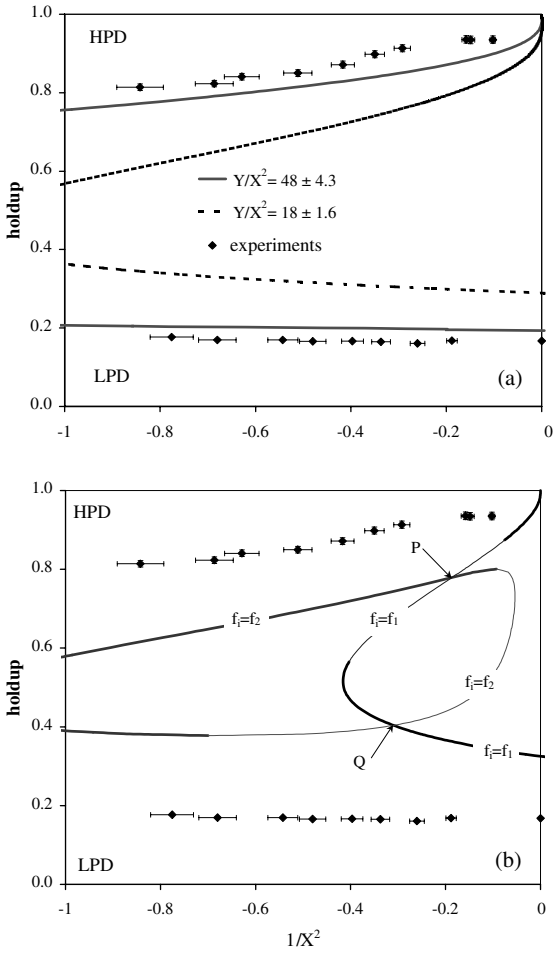

Fig. 6. Comparison of measured holdups for in the HPD and LPD zones with theory for: $\beta = 5.5°$, $Q_1 = 42.5 \pm 2$ ml/min, $\rho_1 = 953.6$ kg/m^3, $\rho_2 = 910.4$ kg/m^3, $\mu = 1.9$ and $\mu_1 = 3.25 \times 10^{-3}$ kg/m/s: (a) TP model, (b) TF model (bold lines—$f_i = f_2$ for $|U_2| > |U_1|$ and $f_i = f_1$ for $|U_1| > |U_2|$).

better when the TF model is applied with $f_i = f_2$. Figs. 7c and 8 show the results of the TF model when the "bridging" suggested in Fig. 6b is applied for improving the TF predictions. Further improvement of the TF model predictions calls for modification of the closure laws used for the friction factors (in particular for τ_i). However, such a modification is out of the scope of the present study. The TP model predictions are also depicted. In general, these figures imply that the best prediction are obtained by the TP model when it is applied with Y calculated based on the same superficial velocity as in pipe flow (denoted in the figures as 'equal U_s').

Due to limitations of the experimental setup, the data in Figs. 5–8 are limited to a relatively small part of the entire flow-rates range where the countercurrent flow is predicted to be feasible. The entire solution domains of the TP and TF models for countercurrent flow are plotted in Fig. 9 (for the same parameters of Fig. 5). Both models indicate the existence of a maximum possible light phase flow rate for a given heavy phase flow rate. At the maximum, the derivative of the light

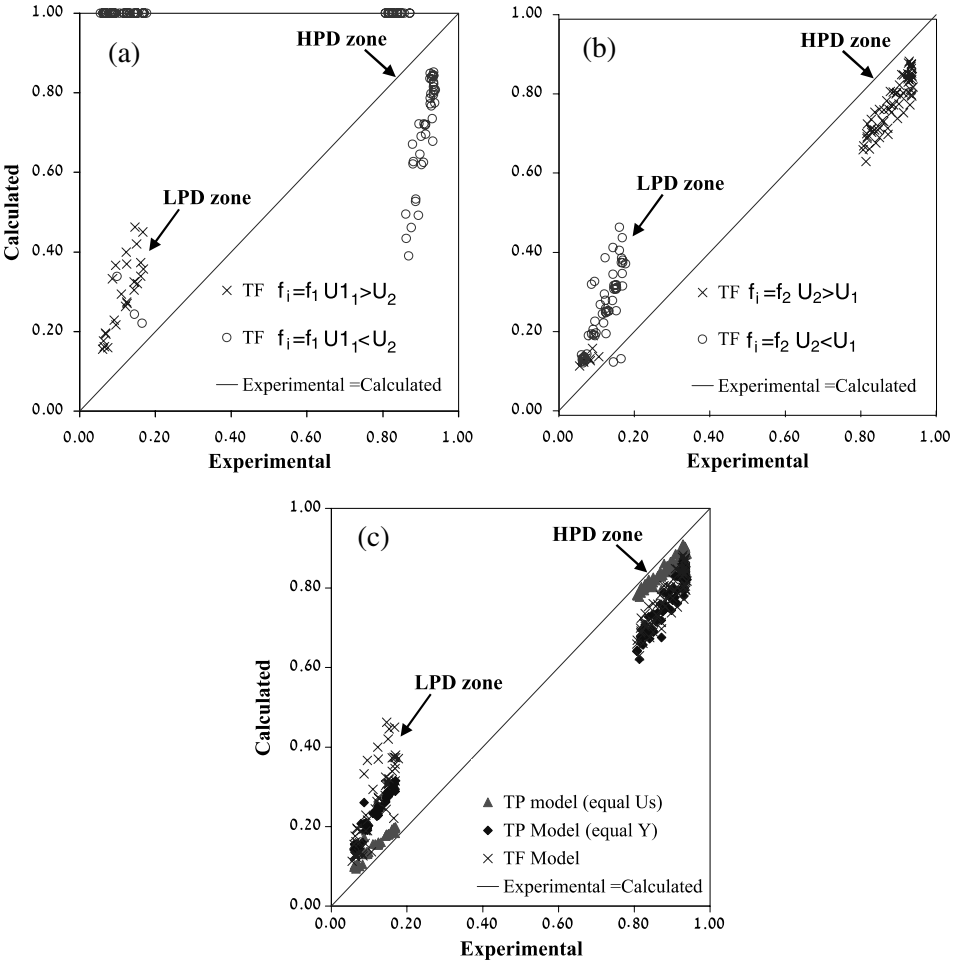

Fig. 7. The holdups as predicted by the TP and TF models vs. experimental data, for $\beta = 5.5°$.

phase flow rate with respect to the holdup vanishes. This point can be considered as the ultimate flooding limit for the stratified flow configuration. A similar condition is widely used to define the flooding limit in spray columns (e.g. Letan, 1988). It is worth noting however, that flooding actually initiates at lower flow rates due to drop entrainment from waves at the interfaces (Ullmann et al., 2001). Fig. 9 demonstrates the variation in the feasible countercurrent domain as predicted by the different models. In particular, the domain predicted via Eq. (15.1) of the TF model ($f_i = f_2$) is significantly wider than that predicted via Eq. (15.2, $f_i = f_1$). This again demonstrates the problematic use of the TF model in the sense of deciding which of the solutions is the relevant one. Therefore, the interpretation of results obtained by TF model should be approached with care.

Fig. 10 shows the dimensionless velocity profiles (normalized with respect to U_{1s}) as predicted via the TP model for three different values of light phase flow rates. In the range of relatively low flow rates, where the experiments were actually conducted (points A and B), the velocity profiles

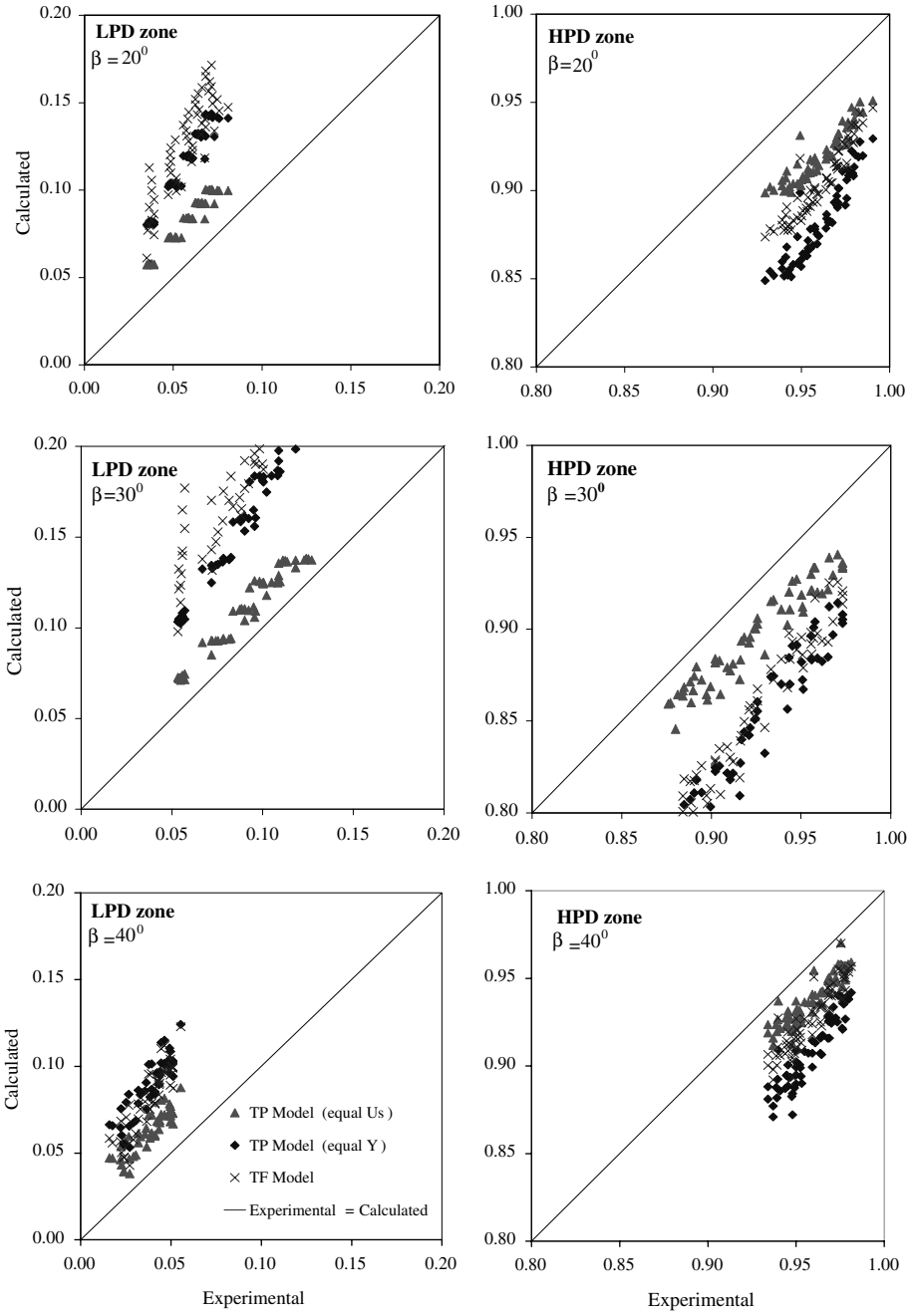

Fig. 8. The holdups as predicted by the TP and TF models vs. experimental data, at various inclination angles.

indicate a significant back-flow in the thicker layer. This is in accordance with the experimental velocity profiles shown in Fig. 11, where in the HPD zone, an upward motion of the heavy liquid

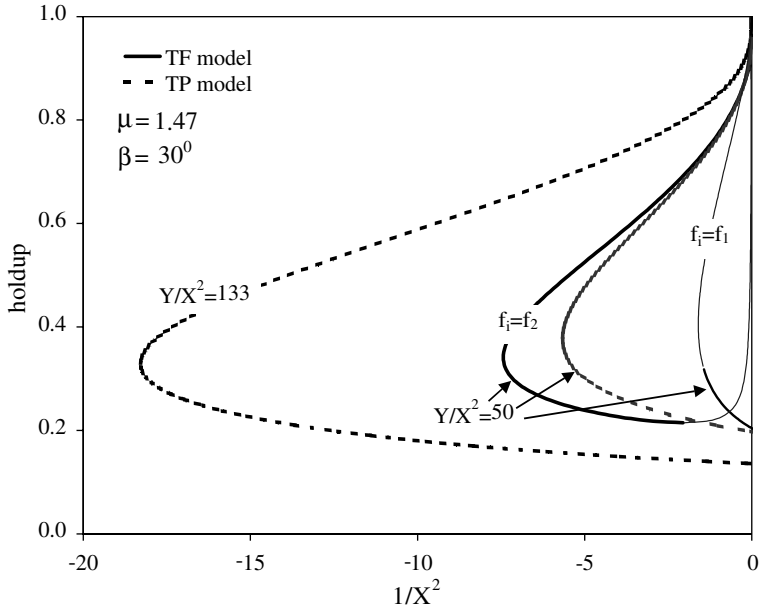

Fig. 9. Entire holdup curve of countercurrent flow predicted by the TP and TF models.

is observed near the interface. Vice versa, a downward flow of the light liquid has been visualized near the interface in the LPD zone (not shown). Fig. 11 shows that the TP model predicts quite reasonably the experimental velocity profile at the centerline of the pipe. Note that the comparison is conducted by plotting the velocity vs. the corresponding area ratio (rather than vs. the corresponding $\tilde{y}$). The largest discrepancy is observed near the liquids' interface and is expected due to different geometries involved. In the pipe, the velocity of the thin layer (where wall effects prevail) must be faster than the corresponding TP model values in order to maintain the same light phase flow rate.

As shown in Fig. 10, at higher flow rates of the light phase, the light phase back-flow in the LPD zone (along the lower branch of the countercurrent solution curve) diminishes. At point C in particular, the velocity at the interface is zero, indicating no back-flow in either of the phases. With a further increase of the light phase flow rate, the backflow is switched to the heavy layer also in the LPD zone. For the system parameters studied in Fig. 10, all HPD modes (upper solution branch) are associated with back-flow in the heavy phase. However, the switch-point C is not always located along the lower branch. For instance for the same $\mu = 1.47$ and for $Y/X^2 < 19.58$, point C is situated on the upper branch of the curve, indicating that backflow of the light phase is possible also with the HPD mode. This issue is further discussed below with reference to Fig. 13. It is worth emphasizing that since the holdup at point E depends on the solution parameters, the HPD (LPD) mode does not necessarily imply higher holdup of the heavy (light) phase.

The effect of the inclination parameter on the holdup curve is demonstrated in Fig. 12a (constant Y/X^2 vs. $1/X^2$) and 12b (constant Y vs. X^2). The former is more convenient for the interpretation of results obtained with constant flow rate of the heavy phase, whereas the latter is

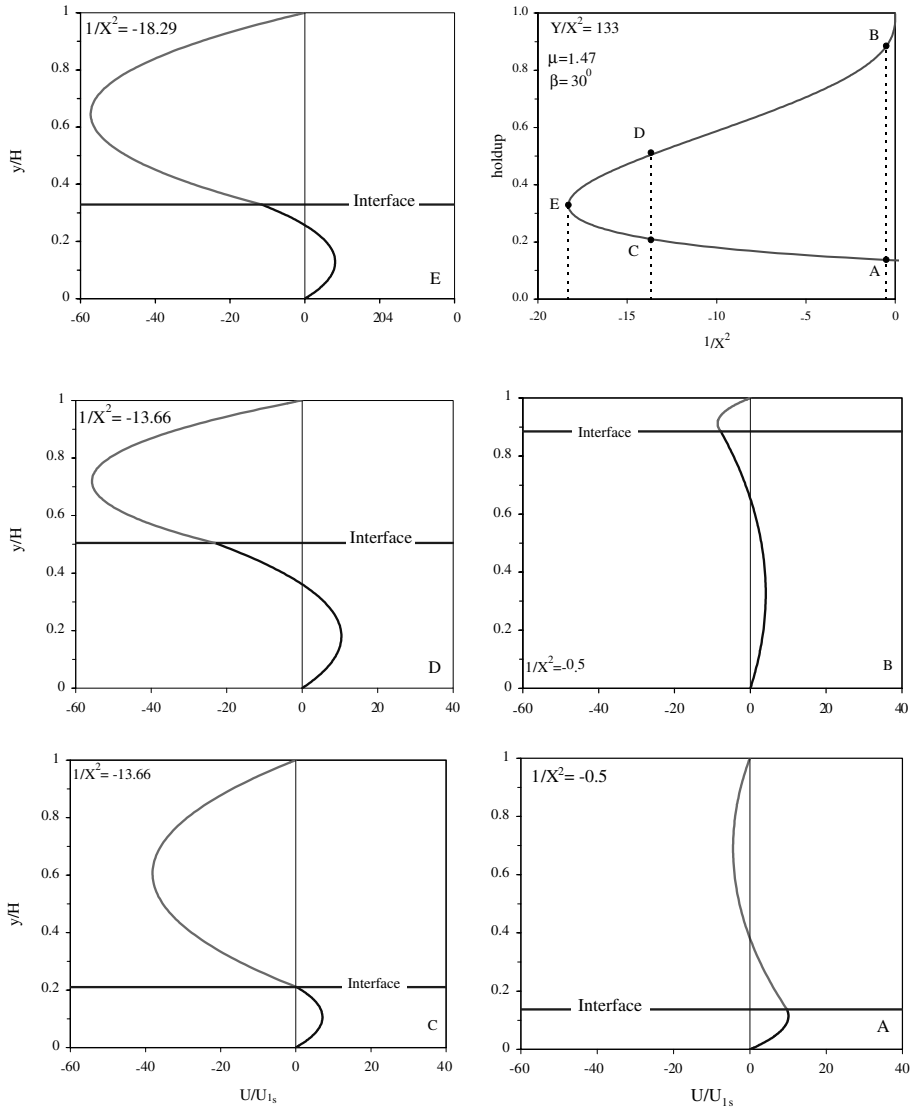

Fig. 10. Velocity profiles along the countercurrent holdup curve as predicted by the TP model.

for constant light phase flow rates. In both cases, increasing the absolute value of the inclination parameter results in a wider feasible range of flow rates for countercurrent flow. Note that solutions for $X^2 = 0$ ($q_1 = 0$) and $\tilde{h} \neq 0$ (see Fig. 12b, for example) do not correspond to a single-phase flow, but to a complete circulation of the heavy phase resulting in a zero net flow. When switching to the co-current region ($X^2 > 0$ and $Y < 0$, the net flow of the heavy phase is upward), these solutions are associated with downward back-flow in the heavy phase.

Fig. 12a and b also show that there is a minimal absolute value of the inclination parameter for which countercurrent flow is feasible ($|Y/X^2| = 5.2$ and $|Y| = 6.35$ for $\mu = 1.47$). The detailed picture of the solutions obtained in the vicinity of $1/X^2 = 0$ in Fig. 12a (or $X^2 = 0$ in Fig. 12b)

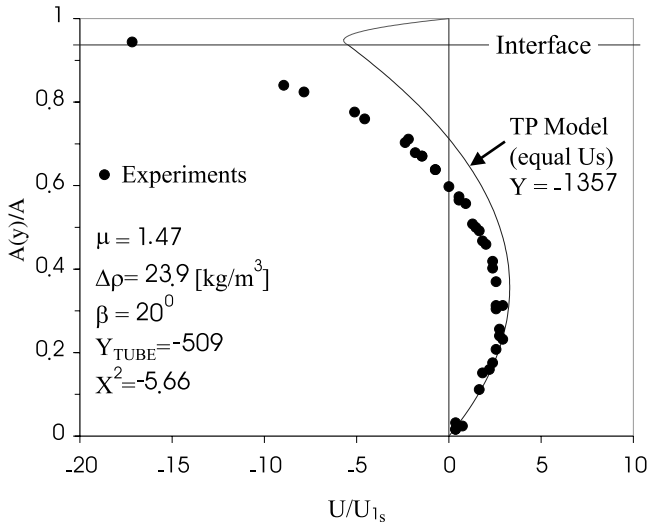

Fig. 11. A comparison between the theoretical and the experimental velocity profiles at the pipe centerline (obtained by a PIV technique) for: $\beta = 20°$, $Q_1 = 17$ ml/min, $\rho_1 = 943.6$ kg/m^3, $\rho_2 = 919.7$ kg/m^3, $\mu = 1.47$ and $\mu_1 = 3.32 \times 10^{-3}$ kg/m/s.

indicates the possible existence of multiple solutions in the co-current flow regime, $X^2 > 0$. The existence of triple solutions to stratified flow models in upward co-current flows ($Y < 0$) has been already discussed in the literature (e.g. Landman, 1991). However, Fig. 12a ($Y/X^2 > 0$) indicates that similarly, triple solutions can be obtained also in downward co-current flows. The multiplicity of solutions for stratified configuration in co-current upward and downward flows is the subject of a following paper (Ullmann et al., 2003).

The effect of the viscosity ratio on the countercurrent solution curve is shown in Fig. 12c. Increasing the viscosity ratio results in an extended range of X^2 for which the flow is feasible. However, it is to be noted that the corresponding range of q diminishes with increasing μ (i.e., for constant Y, higher μ_1 results in lower maximal q_1). The use of X^2 for presenting the solution curves (rather than q) reveals that for $\mu > 100$ or $\mu < 0.01$ the effects of both the viscosity ratio and flow rate ratio, are represented by a single (Martinelli) parameter, whereby the solution parameters space is reduced to two (Y and X^2 only). Fig. 12c also reveals that all curves intersect at a specified X^2. This intersection point corresponds to a zero interfacial velocity. The X^2 of the switch point is determined by Y only and is given by

$$Y = \frac{-(1+\sqrt{-X^2})^4}{\sqrt{-X^2}} = \frac{-1}{\tilde{h}(1-\tilde{h})^3} \tag{17}$$

This relation is shown in Fig. 13 and indicates that for any specified $Y < -9.48$, there are two values of X^2 for which the interfacial velocity is zero. The marked switch-point in Fig. 12c, for example, is the one corresponding to the larger $-X^2$. The other switch-point is associated with very small values of $-X^2$. For $Y > -9.48$ there is no switch point and the back flow is always in the heavy phase.

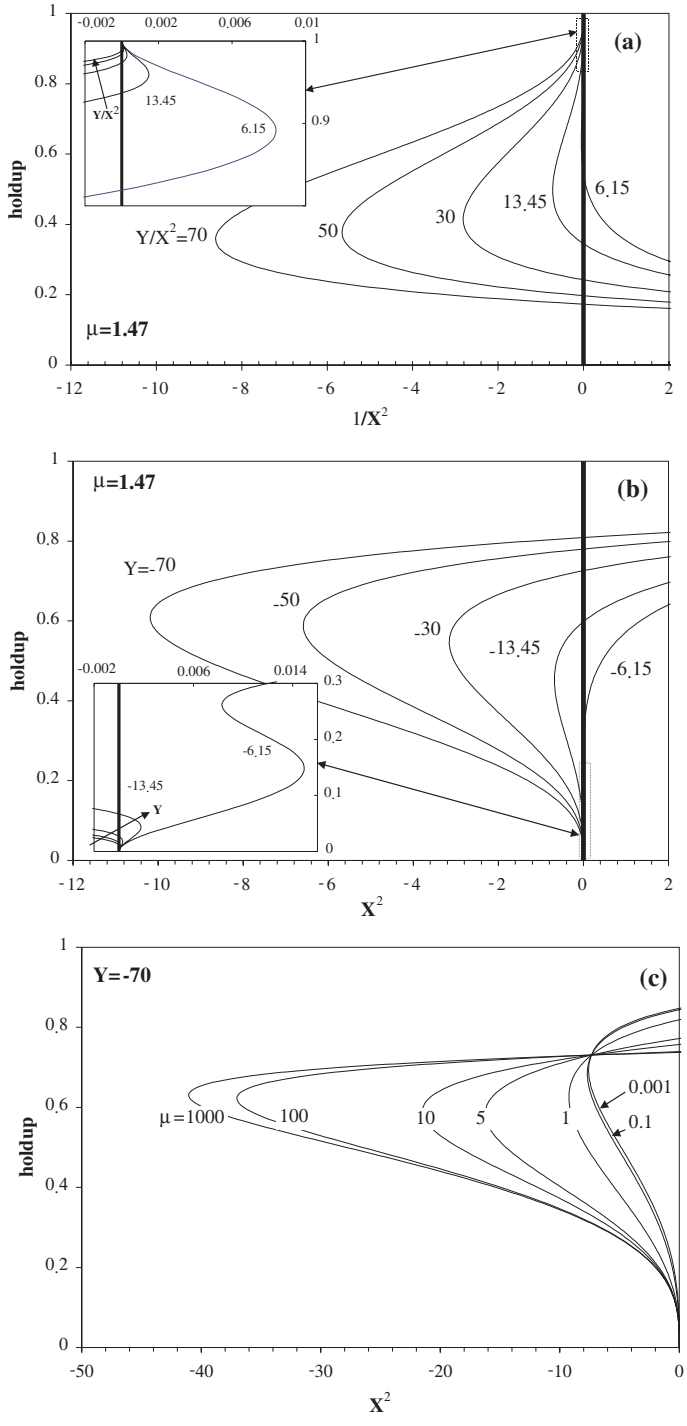

Fig. 12. Effect of model parameters on the holdup curves: (a) Y/X^2, (b) Y, (c) μ.

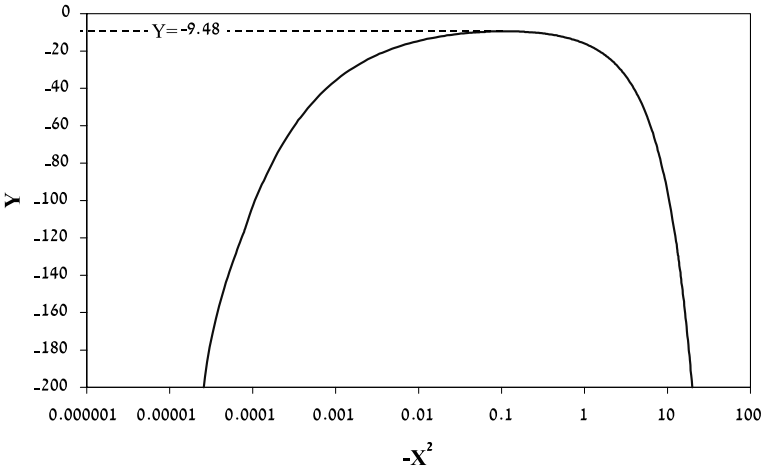

Fig. 13. The location of the switch point (X^2) as determined by Y.

5. Conclusions

Stemming from the premise that the performance of PTE column can be improved by using inclined tubes, a wide experimental study has been conducted for investigating the effect of inclination on the characteristics of liquid–liquid countercurrent flows.

The experiments were conducted with a two-liquid system of a low density difference, $\Delta\rho/\rho_2 \leqslant 0.05$. It was found that even a slight off-vertical inclination of the tube results in a segregation of the liquids. At higher off-vertical inclinations (about 30–40°), a stratified countercurrent flow with a stable interface can be obtained. The experimental results also indicate that two configurations of different holdup are feasible and can coexist in the column.

Simple models, such as the laminar flow between two parallel plates (TP) and the two-fluid (TF) model predict the existence of two configurations of stratified flow. The holdups calculated by the TP model are, generally, in good agreement with the experimental data. On the other hand, the predictions of the TF model are less favorable. Moreover, its application for obtaining the relevant solutions is rather problematic. Using the TF model requires adjustments of the closure laws for the shear stresses and some screening of its various solutions (in some cases up to four solutions can be obtained). This confusion can be avoided by using the TP model. Albeit the different geometry, the TP model provides a better prediction of the holdups. Moreover, it is a convenient tool for conducting a parametric study and for providing insight on the flow phenomena in laminar stratified flows. In particular, the velocity profiles obtained via the TP model indicate a pronounced backflow that can exist in either of the two liquid phases. This finding was verified experimentally by employing the PIV technique for velocity measurements.

The stabilizing effect of inclining the tube can be utilized for increasing the throughput of PTE columns. Preliminary results indicate that by using horizontal settling sections, flooding conditions are postponed and the limiting flow rates increase by a factor of 2–4 (Ullmann et al., 2001).

Acknowledgement

This work was supported by the Ministry of the Environment.

References

Bentwich, M., 1964. Two-phase axial flow in pipe. Trans. ASME, Ser. D 86, 669–672.

Brauner, N., Moalem Maron, D., 1989. Two-phase liquid–liquid stratified flow. Physico-Chem. Hydrodynam. 11, 487–506.

Brauner, N., Rovinsky, J., Moalem Maron, D., 1996. Analytical solution for laminar–laminar two-phase stratified flow in circular conduits. Chem. Eng. Commun. 141–142, 103–143.

Brauner, N., Rovinsky, J., Moalem Maron, D., 1998. A two-fluid model for stratified flows with curved interfaces. Int. J. Multiphase Flow. 24, 975–1004.

Johnston, A.J., 1984. An investigation into the interfacial shear stress contribution in two-phase stratified flow. Int. J. Multiphase Flow 10, 371–383.

Landman, M.J., 1991. Non-unique holdup and pressure drop in two-phase stratified inclined pipe flow. Int. J. Multiphase Flow. 17, 377–394.

Letan, R., 1988. Liquid–Liquid Processes, Chapter 6. In: Kreith, F., Boehm, R.F. (Eds.), Direct Contact Heat Transfer. Springer Verlag, Berlin.

Lo, T.C., Baird, M.H.I., Hanson, C., 1983. Handbook of Solvent Extraction. Wiley-Interscience, New York.

Lockhart, R.W., Martinelli, R.C., 1949. Proposed correlation of data for isothermal two-phae two-component flow in pipes. Chem. Eng. Prog. 45, 39–48.

Robbins, L.A., Roger, W.C., 1997. Liquid–Liquid Extraction. Perry's Chemical Engineers' Handbook, 7th Ed., Sec 15.

Taitel, Y., Dukler, A.E., 1976. A model for predicting flow regime transitions in horizontal and near horizontal gas–liquid flow. AIChE J. 22, 47–55.

Tang, Y.P., Himmelblau, D.M., 1963. Velocity distribution of isothermal two-phase co-current laminar flow in a horizontal rectangular duct. Chem. Eng. Sci. 18, 143–148.

Treybal, R.E., 1963. Liquid Extraction, second ed. McGraw-Hill, New York.

Ullmann, A., Ludmer, Z., Shinnar, R., 1995. Phase transition extraction using solvent mixtures with a critical point of miscibility. AIChE J. 41, 488–500.

Ullmann, A., Ludmer, Z., Shinnar, R., 1997. Novel continuous multistage extraction column based on phase transition of critical-solution mixtures. Chem. Eng. Sci. 52, 567–581.

Ullmann, A., Zamir, M., Ludmer, Z., Brauner, N., 2001. Flow Patterns and Flooding Mechanisms in Liquid–Liquid Countercurrent Flow in Inclined Tubes Proc. of the Third ICMF New Orleans.

Ullmann, A., Zamir, M., Gat, S., Brauner, N., 2003. Multi-Holdups in co-current stratified flow in inclined tubes. Int. J. Multiphase Flow, doi:10.1016/S0301-9322(03)00143-5.

Zamir, M., 2003. An investigation into the flow phenomena in inclined phase transition extraction (PTE) columns based on solvent mixtures with a critical point of miscibility. Ph.D. Thesis, School of Engineering, Tel-Aviv University.